Sensitive Deep Ultraviolet Photodetector and Image Sensor Composed of Inorganic Lead-Free Cs$_3$Cu$_2$I$_5$ Perovskite with Wide Bandgap

Zhi-Xiang Zhang,[‡] Chen Li,[‡] Yu Lu,[‡] Xiao-Wei Tong,[‡] Feng-Xia Liang,*,[†] Xing-Yuan Zhao,[†] Di Wu,[§] Chao Xie,[‡] and Lin-Bao Luo*,[‡]

[‡]School of Electronic Science and Applied Physics and [†]School of Materials Science and Engineering, Anhui Provincial Key Laboratory of Advanced Functional Materials and Devices, Hefei University of Technology, Anhui 230009, China

[§]School of Physics and Engineering and Key Laboratory of Material Physics of Ministry of Education, Zhengzhou University, Zhengzhou, Henan 450052, China

S *Supporting Information*

ABSTRACT: In this work, a sensitive deep ultraviolet (DUV) light photodetector based on inorganic and lead-free Cs$_3$Cu$_2$I$_5$ crystalline film derived by a solution method was reported. Optoelectronic characterization revealed that the perovskite device exhibited nearly no sensitivity to visible illumination with wavelength of 405 nm but exhibited pronounced sensitivity to both DUV and UV light illumination with response speeds of 26.2/49.9 ms for rise/fall time. The I_{light}/I_{dark} ratio could reach 127. What is more, the responsivity and specific detectivity were calculated to be 64.9 mA W^{-1} and 6.9 × 10^{11} Jones, respectively. In addition, the device could keep its photoresponsivity after storage in air environment for a month. It is also found that the capability of Cs$_3$Cu$_2$I$_5$ crystalline film device can readily record still DUV image with acceptable resolution. The above results confirm that the DUV photodetector may hold great potential for future DUV optoelectronic device and systems.
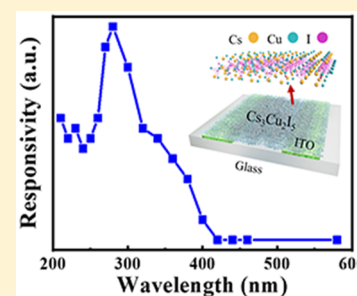
As an important component of the various optoelectronic devices, photodetectors (PDs) have gained tremendous research interest recently owing to their promising applications in light vision, automatic driving, target detection, and iris recognition.[1−4] Unlike visible and infrared light photodetectors, ultraviolet (UV) light detector that can absorb UV photons and convert them into electrical signal is of paramount importance for a number of fields, such as flame detection, secure space-to-space communication, missile guidance, and even space-based warning system.[5] Currently, various high-performance UV photodetectors with different geometries have been developed by using conventional wide-bandgap semiconductors (e.g., zinc oxide, zinc sulfide, gallium oxide, Mg$_x$Zn$_{1−x}$O, III−V compounds, diamond, etc.).[6−11]

Moreover, organolead halide compound with a typical chemical formula of ABX$_3$ has also proved to be an ideal candidate for assembly of highly sensitive UV photodetectors due to its tunable bandgap, ease of processability, and long carrier diffusion length.[12−15] Bakr and his colleagues, for example, have developed a visible-blind UV photodetector using organic MAPbCl$_3$ single crystal.[16] The as-fabricated perovskite photodetector displayed apparent sensitivity to UV irradiation with a swift speed of 24/62 ms (rise/fall time) and a responsivity of 46.9 mA W^{-1}. Moreover, Sargent's group has also reported a sensitive UV photodetector made of crystalline MAPbCl$_3$ film.[17] The responsivity reached 18 A/W, and the response speed was as quick as 1 ms. In spite of this progress,

there is no gainsaying that these organic−inorganic perovskite UV light detectors have usually suffered from severe ambient instability, which constitutes a bottleneck problem for their practical application. To address this issue, people have resorted to other inorganic perovskite materials CsPbX$_3$ (X = Cl, Br, I).[18,19] While this kind of photoelectric material has also proved to be suitable for sensitive photodetector device application, the poisonousness of lead in the material is unfavorable from perspective of environmental protection.

Here, in this study, we reported a highly sensitive UV photodetector by choosing perovskite Cs$_3$Cu$_2$I$_5$ crystalline film with a wide bandgap of 3.8 eV as building block, which is directly deposited on an indium tin oxide (ITO) glass through slow vapor saturation of an antisolvent (VSA) method. It is found that the lead-free Cs$_3$Cu$_2$I$_5$ crystalline film device shows apparent sensitivity to 265 and 365 nm irradiation but is nearly blind to 405 nm visible light. The responsivity is determined to be 60 mA/W, with a response speed of 26.2/49.9 ms for rise/fall time, respectively. More importantly, the as-assembled Cs$_3$Cu$_2$I$_5$ photodetector also exhibits a relatively good ambient stability even after storage in ambient condition for a month. Lastly, it is also revealed that the Cs$_3$Cu$_2$I$_5$ crystalline film device can function as a UV light image sensor, which can
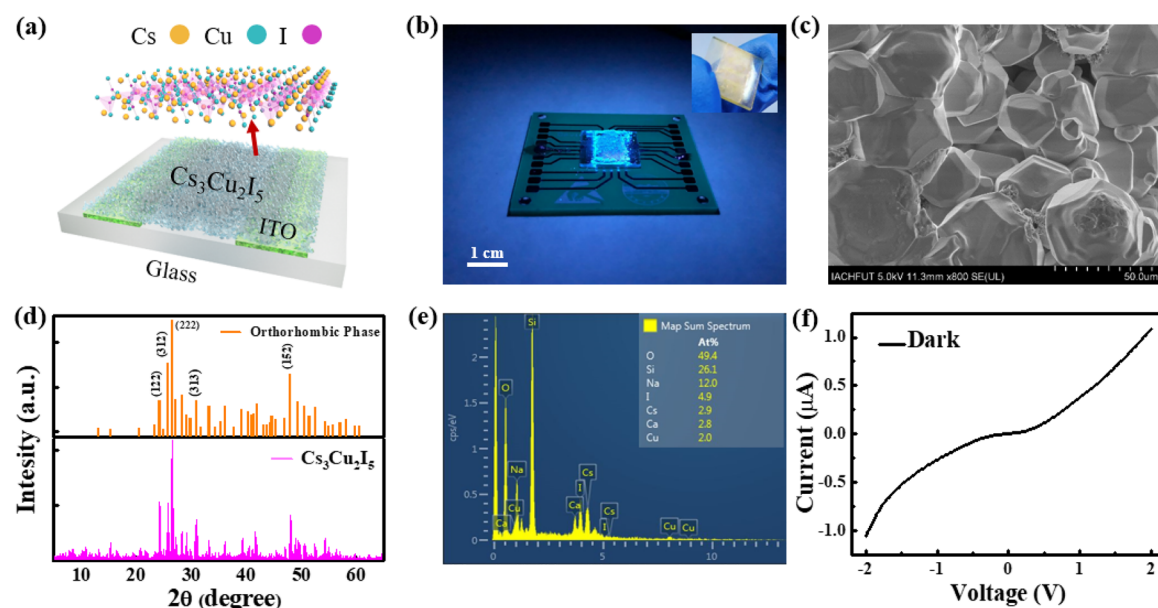
**Figure 1.** (a) Schematic of the DUV device and the crystal structure of the $Cs_3Cu_2I_5$. (b) Digital camera photograph of the DUV photodetector shined by 265 nm light. (inset) The DUV photodetector under white light. (c) FESEM study of the $Cs_3Cu_2I_5$ sample. (d) X-ray diffraction characterization of the $Cs_3Cu_2I_5$ and the standard date. (e) EDS analysis of the $Cs_3Cu_2I_5$ sample on glass. (f) $I-V$ curve of the $Cs_3Cu_2I_5$ film photodetector without any light illumination.
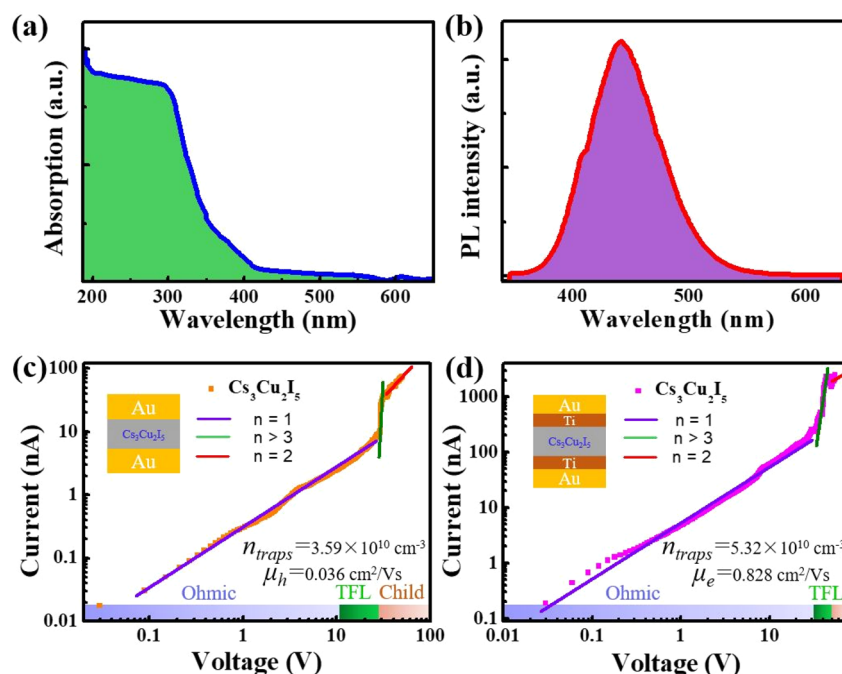

Figure 2. (a) Light absorption spectrum of the perovskite crystalline film. (b) The steady-state PL spectrum of the film. (c) $I-V$ curve of a hole-only device. (inset) The corresponding device geometry. (d) $I-V$ curve for an electron-only device. (inset) The corresponding device geometry.

readily record both UV and deep ultraviolet (DUV) light images with acceptable resolution. The above study suggests that the wide bandgap perovskite photodetector may find potential applications in next-generation UV optoelectronic systems.

The geometry of the $Cs_3Cu_2I_5$ crystalline film DUV photodetector (DUVPD) is portrayed in Figure 1a. In this work, the perovskite crystalline film was directly grown on ITO glass by a modified antisolvent vapor-assisted crystallization process.[20] For convenience, the ITO glass was predefined with 50 μm wide channel before the growth of perovskite crystalline

film (Please refer to the Figure S1). In the crystal structure of $Cs_3Cu_2I_5$, the $[Cu_2I_5]^{3-}$ is composed of a tetrahedral and trigonal planar Cu halide units, with two kinds of structure isolated by Cs^+ ions.[21,22] Figure 1b shows the digital camera photograph of the perovskite photodetector shined by 265 nm illumination. Clearly, the $Cs_3Cu_2I_5$ material exhibits obvious photoluminescence, suggesting the unique optical or photoelectric property. From the vertical view field emission scanning electron microscopy (FESEM) image in Figure 1c and Figure S2a,b, one can easily conclude that the diameter of the single crystals ranges from 5 to 50 μm, with an average
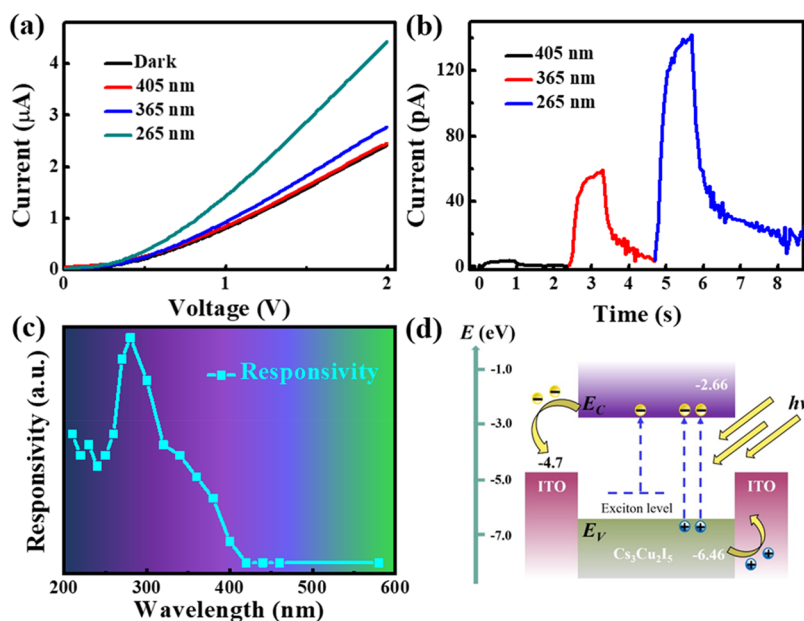
Figure 3. (a) $I-V$ curves of the device shined with various wavelengths; the power intensities are all set to be 2.74 mW cm^{-2}. (b) Photoresponse curves of the DUV device illuminated by various wavelengths. (c) The spectral response of the perovskite photodetector. (d) The energy band diagram under light illumination.

value of 40 μm (Figure S2c). Further X-ray diffraction (XRD) pattern shown in Figure 1d shows that the Cs$_3$Cu$_2$I$_5$ sample could be attributed to orthorhombic phase (a = 10.113 Å, b = 11.624 Å, c = 14.367 Å, PDF No. 45-0077). Energy-dispersive X-ray spectroscopy (EDS) analysis also finds that the Cs/Cu/I ratio is ~3:2:5 (Figure 1e), consistent with the stoichiometric ratio of Cs$_3$Cu$_2$I$_5$. According to the current−voltage ($I-V$) characteristic in Figure 1f, a clear nonlinear $I-V$ curve was observed, which means Schottky barrier was formed at Cs$_3$Cu$_2$I$_5$/ITO interface.

Figure 2a shows the absorption spectra of the wide bandgap Cs$_3$Cu$_2$I$_5$ crystalline film, from which obvious absorption edge at ~330 nm was observed. This result coincides with its bandgap of 3.8 eV. Nonetheless, to our surprise, from the steady-state photoluminescence (PL) spectrum analysis in Figure 2b, the emission peak of Cs$_3$Cu$_2$I$_5$ crystalline film is estimated to be at 442 nm. This emission peak is inconsistent with the bandgap estimated from the absorption, signifying that the PL spectrum should not be simply ascribed to a direct-band emission process. As observed in other zero-dimensional (0D) Sn-based metal halide perovskites,[23] this difference between the emission peak and the absorption edge (Stokes shift ≈ 112 nm) was probably caused by the Jahn−Teller distortion and self-trapped excitons, as a consequence of the change of electronic configuration of the Cu atoms from 3d^{10} to 3d^9 after Cs$_3$Cu$_2$I$_5$ absorbed the photon energy.[21,24]

To further explore the carrier transport characteristics of the Cs$_3$Cu$_2$I$_5$ single crystals by using the space charge limited current (SCLC) approach, we then fabricated both electron-only and hole-only devices.[25−29] The $I-V$ characteristics for both devices are apparently composed of three regions, as displayed in Figure 2c,d. At low bias voltage, the relationship between the current (I) and voltage (V) is linearly ohmic. However, as the applied voltage increases, the incident carriers will fill the trap states. The limit voltage V_{TFL} can be calculated by trap-state density (n_{traps}), as described by the following equation

$$V_{TFL} = \frac{e n_{traps} d^2}{2 \varepsilon_0 \varepsilon} \tag{1}$$

where ε_0 is the vacuum permittivity, d is the thickness of the sample (1.5 mm), e is the elementary electronic charge, and the relative dielectric constant (ε = 32.5) of Cs$_3$Cu$_2$I$_5$ is calculated according to the following formula

$$\varepsilon = \frac{cd}{\varepsilon_0 A} \tag{2}$$

where d is the thickness of the sample, and A is the surface area (6.25 mm^2). On the basis of these values, the capacitance of the as-prepared perovskite is estimated to be 1.2 pf by using an impedance analyzer. When the applied voltage is further increased, both devices will work in the SCLC Child's regime. In this condition, the dark current of the perovskite can be determined by the Mott−Gurney law

$$J_D = \frac{9 \varepsilon_0 \varepsilon \mu V_b^2}{8 d^3} \tag{3}$$

where V_b is the bias voltage, ε is the relative dielectric constant of the Cs$_3$Cu$_2$I$_5$, d is the thickness of the single crystal, J_D is the current without light illumination, and μ is the hole or electron mobility, respectively. On the basis of the two formulas, the hole trap density (n_{traps}) and hole mobility (μ_h) are determined to be 3.58 × 10^{10} cm^{-3} and 0.036 cm^2/(V s), respectively. What is more, with regard to the electron-only device, the electron trap density (n_{traps}) and electron mobility (μ_e) are estimated to be 5.32 × 10^{10} cm^{-3} and 0.828 cm^2/(V s), respectively. Compared with other perovskite materials including CH$_3$NH$_3$PbBr$_3$ (hole mobility is 164 cm^2/(V s), electron mobility is 24.8 cm^2/(V s))[25] and Cs$_2$AgBiBr$_6$ (carrier mobility is 3.17 cm^2/(V s)),[29] the carrier mobility of the present Cs$_3$Cu$_2$I$_5$ is rather low, which is probably due to the relatively large binding energy.[21]

Even though the carrier mobility is relatively low, the perovskite crystalline film exhibits obvious photoresponse
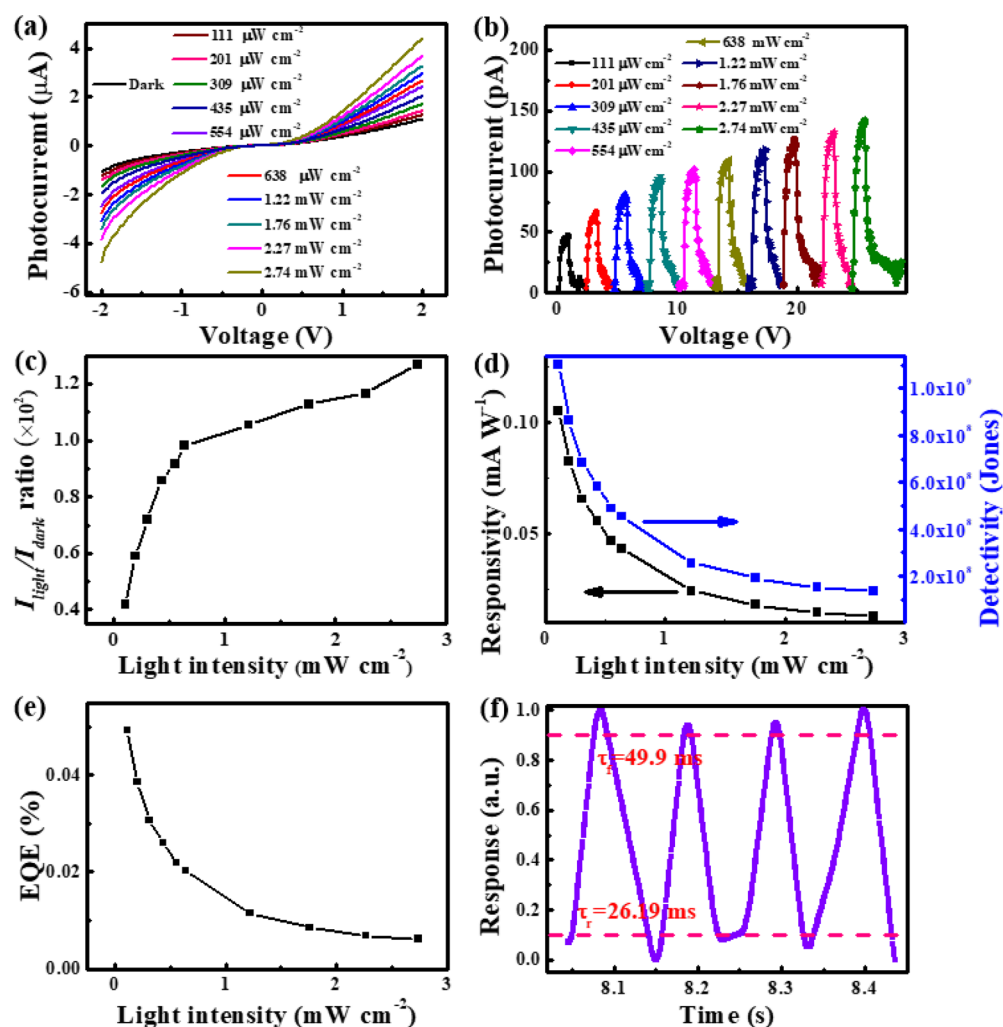
Figure 4. (a) Current–voltage characteristics of the perovskite film device under 265 nm irradiation with varied intensities. (b) Response curve of the perovskite device under 265 nm irradiation with various intensities. (c) I_{light}/I_{dark} ratio at various light intensities. (d) Responsivity and detectivity of the DUV photodetector at various light intensities. (e) Dependence of EQE upon intensity at zero voltage. (f) Response curve of the perovskite DUV device under pulsed 265 nm irradiation with a frequency of 20 Hz.

when shined with light illumination (Figure 3a). Figure 3b exhibits the time-dependent photoresponse under different light irradiation (265, 365, 405 nm) at zero bias. Clearly the perovskite UV device is sensitive to 265 and 365 nm light, but it is virtually blind to 405 nm light. The rejection ratio, which is defined as the photocurrent under 265 nm light illumination over the photocurrent under 405 nm light illumination, was calculated to be 17.8. Such a spectral selectivity is also confirmed by the normalized spectral selectivity, as shown in Figure 3c. To understand the above photosensitivity, the energy band diagram was provided in Figure 3d. For the $Cs_3Cu_2I_5$ perovskite film, the lowest unoccupied molecular orbital (LUMO) and highest occupied molecular orbital (HOMO) values are −2.66 and −6.46 eV,[18] respectively. When illuminated by photons with energy larger than the band gap of $Cs_3Cu_2I_5$ (3.8 eV), photogenerated excitons will be formed in perovskite. Like conventional Schottky junction, the electron–hole pairs are swiftly discomposed in build-in electric field, forming photocurrent in the circuit. Furthermore, the photoresponse to illumination with energy lower than the band gap is possibly caused by the existence of exciton levels, in which the excitons will decompose into free electrons and

holes through thermal energy or other energies and lead to the generation of photocurrents.[24]

In addition to light wavelength, the photoresponse of the perovskite device was also found to strongly depend upon the intensity of the incident illumination. Figure 4a plots the current–voltage curves under 265 nm with different intensities. It is observed that, when the incident light intensity increases from 111 to 2.74 mW/cm⁻², the photocurrent will gradually increase from 41 to 140 pA (Figure 4b), as a result of more photoexcited charge carriers generated at higher intensity. The corresponding on/off ratio, which is defined by the photocurrent/dark current, was also observed to increase linearly with the increase of DUV intensity. When the incident light intensity reaches 2.74 mW/cm⁻², the on/off ratio will reach a maximum value of 142. To assess the present perovskite device quantitatively, several important parameters including on/off ratio (I_{light}/I_{dark}), responsivity (R), specific detectivity (D), and external quantum efficiency (EQE) could be estimated by the following equations[30−32]

$$R = \frac{I_{light} - I_{dark}}{P_{light}S} \tag{4}$$
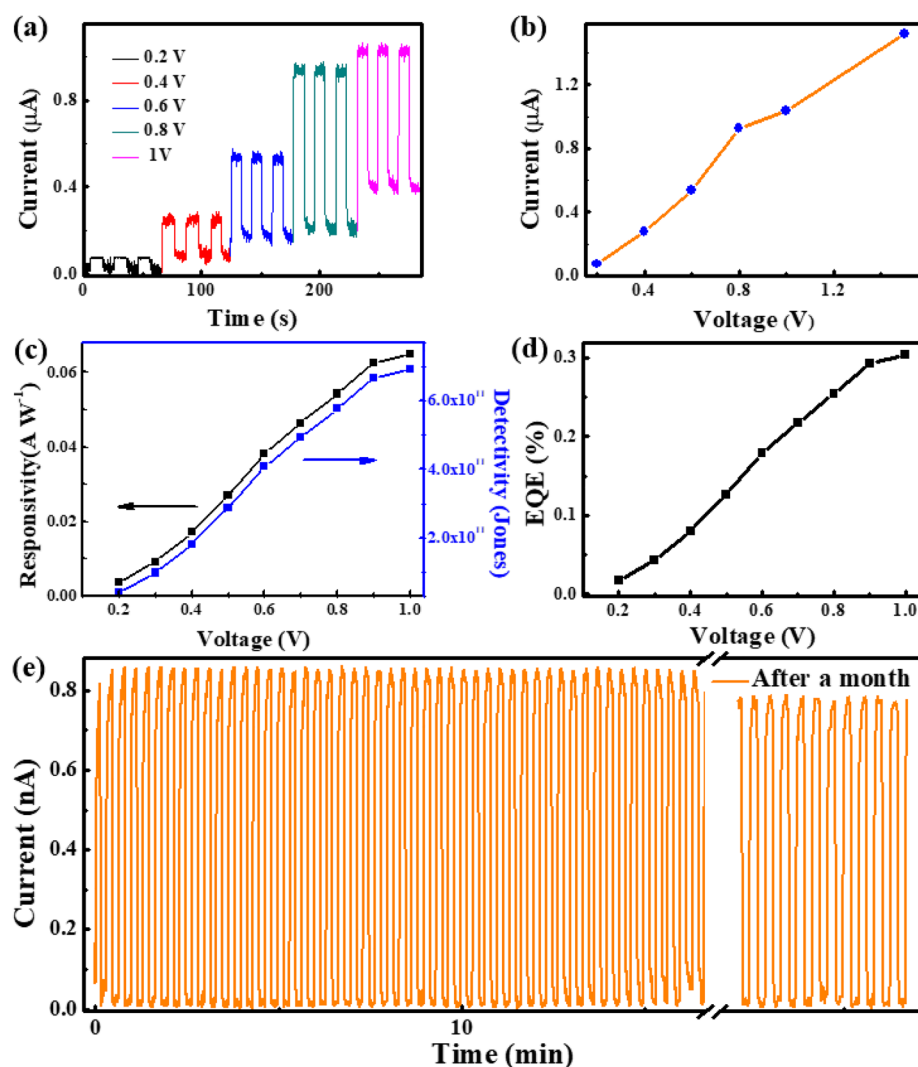
Figure 5. (a) Bias voltage-dependent photoresponse of the perovskite photodetector udder 265 nm irradiation. (b) Relationship between the photocurrent of the perovskite photodetector with different bias voltages. (c) R and D^* at varied bias voltages. (d) EQE of the device at varied bias voltages. (e) Photoresponse of the device for 50 cycles; another 10 cycles were tested after storage in air for a month.

$$D = \frac{R_{light}S^{1/2}}{(2eI_{dark})^{1/2}} \quad (5)$$

$$EQE = R\frac{hc}{e\lambda} \quad (6)$$

where I_{light} is the current under light irradiaton, I_{dark} is the current without light illumination (1.1 pA), P_{light} is the incident light intensity, S is the effective size of the perovskite photodetector (3.5×10^{-3} cm^{-2}), e is the elementary charge, h is the Planck's constant, c is the speed of light, and λ is the incident light wavelength (265 nm), respectively. By using these constant and values, the R, D, and EQE under various light intensities are estimated. As plotted in Figure 4c−e, all three parameters reach the highest values of 0.11 mA W^{-1} (R), 1.1×10^9 Jones (D), and 0.05% (EQE) under 265 nm DUV irradiation with a weak intensity of 111 μW cm^{-2}, respectively. Nonetheless, with increasing DUV light intensity, the three metrics will decrease. This kind of phenomenon is associated with the self-heating effect in device at high illumination intensity, which may result in the increases of carrier scatting and recombination probability.[30,33] To estimate the response speed of perovskite photodetector, the photoresponse to switchable light illumination was then studied. Figure 4f shows the photoresponse under repeatable 265 nm light illumination. Clearly, the response curve has well-defined rising and decaying edges. When the frequency was at 20 Hz, the perovskite photodetector can still be easily converted between on and off states, with rise/fall times of 26.19/49.9 ms. Such a response speed could be further improved by either enhancing the applied voltage or improving the quality of perovskite crystalline film.

As a matter of fact, the bias voltage applied on perovskite film device can also influence the photocurrent. Figure 5a exhibits the photocurrent at different bias voltages under the same DUV illumination. The photocurrent was found to increase from 7.6×10^{-8} to 1.5×10^{-6} A as the applied bias increases from 0.2 to 1.5 V (Figure 5b). This finding is reasonable, as the separation efficiency will be enhanced, and the photogenerated carriers recombination will be restrained at large bias voltage. After a careful comparison of the responsivity, the detectivity, and EQE at various applied voltages, one may find that all three metrics rise substantially with rising bias voltage (Figure 5c,d). Specifically, at 1 V, the

Table 1. Comparison of the Device Parameters of Our Photodetector and Other DUVPDs in Literature

device structure	wavelength (nm)	R [mA W^{-1}]	dark current (pA)	τ_r/τ_f	ref
ITO−Cs$_3$Cu$_2$I$_5$−ITO	265	64.9	1.1	26.2/49.9 ms	this work
graphene/β-Ga$_2$O$_3$	254	3.9×10^4	1.1×10^6	84.8/219.2 s	34
CsPbX3 QDs/a-Si	200	54		0.48/1.03 ms	35
GQD	254	2.1	1.5	64/43 ms	36
Au−Ga$_2$O$_3$ nanowires	254	0.01	10	10/3 ms	37
ZnS	265	0.1	0.01	350/70 ms	38
Ga$_{1.8}$Sn$_{0.2}$O$_3$	254	17.9	1200	7.3/5.12 s	39

responsivity, detectivity, and EQE were 64.9 mA W^{1-}, 6.9 × 10^{11} Jones, and 0.3%, respectively. Another important feature that is worth discussing is that the present perovskite film UV device has very good device stability, which is unusual in the majority of perovskite materials-based optoelectronic devices. Figure 5e compares the photoresponse of perovskite film device before and after the perovskite UV detector was stored for a month. The device retained its photoresponse properties with only 7% degradation in photocurrent. Such good device stability is ascribed to the unusual structure of perovskite material, in which the [Cu$_2$X$_5$]$^{3-}$ is wrapped and protected by the Cs$^+$, leading to the spatial isolation of [Cu$_2$X$_5$]$^{3-}$ from the oxygen and moisture. By this token, the perovskite material virtually keeps unchanged after long-time storage (Figure S3).

In general, most of the perovskite could be directly grown by one-step spin-coating method, and the as-prepared material often displayed outstanding optoelectronic characteristics. To unveil the difference between the present Cs$_3$Cu$_2$I$_5$ crystalline film and Cs$_3$Cu$_2$I$_5$ film obtained directly by spin-coating method, two Cs$_3$Cu$_2$I$_5$ photodetectors assembled by different methods were then fabricated, and their device performance was compared. The schematic of the film photodetector was provided in Figure S4a. Figure S4b,c displays the photoresponse under 265 nm irradiation of 2.74 mW cm^{-2}. Compared with the device based on the above crystalline film, the device made of spin-coated perovskite film exhibited weaker photoresponse. Specifically, when the applied voltage was as high as 20 V, the responsivity was estimated to be 0.94 mA W^{-1}, nearly 70 times lower than that of perovskite crystalline film detector. Such inferior device performance is likely correlated with the inferior material quality, as unveiled by the atomic force microscope (AFM) image (Figure S4d).

Table 1 compares the key device metrics of the our DUV device and other DUV photodetectors made of either perovskite materials or conventional ultrawide bandgap semiconductors. Apparently, the responsivity of the present device is lower than that of graphene/β-gallium oxide wafer,[34] but it is larger than previously reported devices assembled from CsPbX$_3$ QDs/a-Si,[35] graphene quantum dots (GQD),[36] Au−Ga$_2$O$_3$ nanowires,[37] ZnS,[38] and Ga$_{1.8}$Sn$_{0.2}$O$_3$.[39] Furthermore, the dark current of this perovskite detector is smaller than the majority of photodetectors listed in the table. Such a relatively small dark current shall be associated with the high exciton binding energy. It is also worth mentioning that, thanks to the efficient charge separation of the ITO-Cs$_3$Cu$_2$I$_5$ interface, the corresponding response speed of our photodetector is faster than most of the DUVPDs. This relatively fast response speed, along with low dark current, high responsivity, and good ambient stability, makes this perovskite film device highly likely for future DUV optoelectronic devices.

To explore the possibility of this DUVPD for other optoelectronic devices, light image sensing was then performed. Figure 6a illustrates the schematic of the instrument for imaging characterization. During the image-sensing
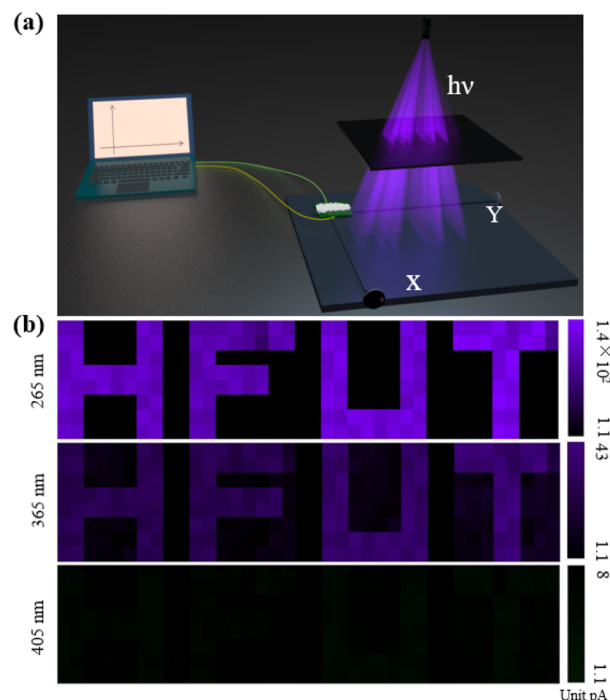

Figure 6. (a) Schematic illustration of the setup for recording DUV image. (b) The image-sensing profile of HFUT under 265, 365, and 405 nm light excitation.

process, three different images were produced by shining DUV (265 nm)/UV (365 nm)/visible (405 nm) light directly on a mask with an "HFUT" (HFUT = Hefei University of Technology) pattern. The perovskite will move along both x- and y-axes to collect the photocurrent in each pixel, and all the photocurrent corresponding pixels will be sent to the imaging software. Figure 6b shows the photocurrent mapping profile under illumination of 265, 365, and 405 nm. Clearly, the purple image and light purple image of the HFUT pattern under 265 and 365 nm illumination can be readily formed in Figure 6b. However, when the wavelength was replaced with 405 nm, no HFUT image can be observed. As a matter of fact, more complicated image sensing with relatively large pixels can be also achieved (Figure S5), suggesting that the perovskite film device is suitable for DUV light image sensing application.

In conclusion, we have fabricated a DUV light detector by using all-inorganic, lead-free, and wide-bandgap Cs$_3$Cu$_2$I$_5$ perovskite crystalline film, which was prepared by a solution-based growth method. Optoelectronic analysis revealed that the perovskite device showed nearly no sensitivity to visible illumination but exhibited pronounced sensitivity to 365 nm

UV and 265 nm DUV light with response speeds of 26.2/49.9 ms for rise/fall times. The responsivity and EQE were as high as 64.9 mA W^{-1} and 0.3%, respectively. It is also found that the current new DUVPD can also function as efficient image sensor that can readily collect DUV image with acceptable resolution. These results, along with the good ambient stability, testify that the present $Cs_3Cu_2I_5$ crystalline film DUV photodetector possesses great potential application for next-generation optoelectronic devices.

ASSOCIATED CONTENT

Ⓢ Supporting Information

The Supporting Information is available free of charge on the ACS Publications website at DOI: 10.1021/acs.jp-clett.9b02390.

Schematic illustration of setup for growing the $Cs_3Cu_2I_5$, FESEM images, statistical distribution of single-crystal diameters, XRD patterns before and after storage for one month, the method for fabricating the $Cs_3Cu_2I_5$ film photodetector, schematic illustration of $Cs_3Cu_2I_5$ film PD, I−V curves, I−T curves (PDF)

AUTHOR INFORMATION

Corresponding Authors
*E-mail: fxliang@hfut.edu.cn. (F.-X.L.)
*E-mail: luolb@hfut.edu.cn. (L.-B.L.)

ORCID Ⓞ
Di Wu: 0000-0003-3266-0612
Chao Xie: 0000-0003-4451-767X
Lin-Bao Luo: 0000-0001-8651-8764

Notes
The authors declare no competing financial interest.

ACKNOWLEDGMENTS

REFERENCES

(1) Wang, Z.; Safdar, M.; Jiang, C.; He, J. High-Performance UV−Visible−NIR Broad Spectral Photodetectors Based on One-Dimensional In$_2$Te$_3$ Nanostructures. *Nano Lett.* **2012**, *12*, 4715−4721.

(2) Gan, X.; Shiue, R.; Gao, Y.; Meric, I.; Heinz, T.; Shepard, K.; Hone, J.; Assefa, S.; Englund, D. Chip-Integrated Ultrafast Graphene Photodetector with High Responsivity. *Nat. Photonics* **2013**, *7*, 883−887.

(3) Zhou, X.; Hu, X. Z.; Zhou, S. S.; Song, H. Y.; Zhang, Q.; Pi, L. J.; Li, H. Q.; Lu, J. T.; Zhai, T. Y.; Li, L. Tunneling Diode Based on WSe$_2$/SnS$_2$ Heterostructure Incorporating High Detectivity and Responsivity. *Adv. Mater.* **2018**, *30*, 1703286.

(4) Zhuo, R.; Wu, D.; Wang, Y.; Wu, E.; Jia, C.; Shi, Z.; Xu, T.; Tian, Y.; Li, X. A Self-Powered Solar-Blind Photodetector based on a MoS$_2$/b-Ga$_2$O$_3$ Heterojunction. *J. Mater. Chem. C* **2018**, *6*, 10982−10986.

(5) Deng, W.; Zhang, X.; Huang, L.; Xu, X.; Wang, L.; Wang, J.; Shang, Q.; Lee, S. T.; Jie, J. Aligned Single-Crystalline Perovskite Microwire Arrays for High-Performance Flexible Image Sensors with Long-Term Stability. *Adv. Mater.* **2016**, *28*, 2201−2208.

(6) Li, M.; Zhou, S.; Wang, R.; Yu, Y.; Wong, H.; Luo, Z.; Li, H.; Gan, L.; Zhai, T. Y. In Situ Formed Nanoparticle-Assisted Growth of Large-Size Single Crystalline h-BN on Copper. *Nanoscale* **2018**, *10*, 17865−17872.

(7) Zhou, Z.; Lan, C.; Yip, S.; Wei, R.; Li, D.; Shu, L.; Ho, J. C. Towards High-Mobility InGaO Nanowire Field-Effect Transistors. *Nano Res.* **2018**, *11*, 5935−5945.

(8) Wang, F.; Song, L.; Zhang, H.; Meng, Y.; Luo, L.; Xi, Y.; Liu, L.; Han, N.; Yang, Z.; Tang, J.; Shan, F.; Ho, J. C. ZnO Nanofiber Thin-Film Transistors with Low-Operating Voltages. *Adv. Electron. Mater.* **2018**, *4*, 1700336.

(9) Han, J.; Wang, J.; Yang, M.; Kong, X.; Chen, X.; Huang, Z.; Guo, H.; Gou, J.; Tao, S.; Liu, Z.; Wu, Z.; Jiang, Y.; Wang, X. Graphene/Organic Semiconductor Heterojunction Phototransistors with Broad-band and Bi-directional Photoresponse. *Adv. Mater.* **2018**, *30*, 1804020.

(10) Xie, C.; Lu, X. T.; Tong, X. W.; Zhang, Z. X.; Liang, F. X.; Liang, L.; Luo, L. B.; Wu, Y. C. Recent Progress in Solar-Blind Deep-Ultraviolet Photodetectors Based on Inorganic Ultrawide Bandgap Semiconductors. *Adv. Funct. Mater.* **2019**, *29*, 1806006.

(11) Wang, F.; Gao, T.; Zhang, Q.; Hu, Z.; Jin, B.; Li, L.; Zhou, X.; Li, H.; Van Tendeloo, G.; Zhai, T. Y. Liquid-Alloy-Assisted Growth of 2D Ternary Ga$_2$In$_4$S$_9$ toward High-Performance UV Photodetection. *Adv. Mater.* **2019**, *31*, 1806306.

(12) Dou, L.; Yang, Y.; You, J.; Hong, Z.; Chang, W.; Li, G.; Yang, Y. Solution-Processed Hybrid Perovskite Photodetectors with High Detectivity. *Nat. Commun.* **2014**, *5*, 5404.

(13) Zhao, Y.; Zhu, K. Organic-Inorganic Hybrid Lead Halide Perovskites for Optoelectronic and Electronic Applications. *Chem. Soc. Rev.* **2016**, *45*, 655.

(14) Dirin, D. N.; Cherniukh, I.; Yakunin, S.; Shynkarenko, Y.; Kovalenko, M. Solution-Grown CsPbBr$_3$ Perovskite Single Crystals for Photon Detection. *Chem. Mater.* **2016**, *28*, 8470−8474.

(15) Chen, Q.; De Marco, N.; Yang, Y.; Song, T.; Chen, C.; Zhao, H.; Hong, Z.; Zhou, H.; Yang, Y. Under the Spotlight: The Organic-inorganic Hybrid Halide Perovskite for Optoelectronic Applications. *Nano Today* **2015**, *10*, 355−396.

(16) Maculan, G.; Sheikh, A.; Abdelhady, A.; Saidaminov, M.; Haque, M.; Murali, B.; Alarousu, E.; Mohammed, O. F.; Wu, T.; Bakr, O. M. CH$_3$NH$_3$PbCl$_3$ Single Crystals: Inverse Temperature Crystallization and Visible-Blind UV-Photodetector. *J. Phys. Chem. Lett.* **2015**, *6*, 3781−3786.

(17) Adinolfi, V.; Ouellette, O.; Saidaminov, M.; Walters, G.; Abdelhady, A.; Bakr, O. M.; Sargent, E. H. Fast and Sensitive Solution-Processed Visible-Blind Perovskite UV Photodetectors. *Adv. Mater.* **2016**, *28*, 7264−7268.

(18) Li, Y.; Shi, Z.; Lei, L.; Ma, Z.; Zhang, F.; Li, S.; Xu, T.; Li, X.; Shan, C.; Du, G.; Wu, D. Controllable Vapor-Phase Growth of Inorganic Perovskite Microwire Networks for High-Efficiency and Temperature-Stable Photodetectors. *ACS Photonics* **2018**, *5*, 2524−2532.

(19) Shoaib, M.; Zhang, X.; Wang, X.; Zhou, H.; Xu, T.; Wang, X.; Hu, X.; Liu, H.; Fan, X.; Zheng, W.; Yang, T.; Yang, S.; Zhang, Q.; Zhu, X.; Sun, L.; Pan, A. Directional Growth of Ultralong CsPbBr$_3$ Perovskite Nanowires for High-Performance Photodetectors. *J. Am. Chem. Soc.* **2017**, *139*, 15592−15595.

(20) Saidaminov, M. I.; Adinolfi, V.; Comin, R.; Abdelhady, A. L.; Peng, W.; Dursun, I.; Yuan, M.; Hoogland, S.; Sargent, E. H.; Bakr, O. M. Planar-integrated Single-crystalline Perovskite Photodetectors. *Nat. Commun.* **2015**, *6*, 8724.

(21) Jun, J.; Sim, K.; Iimura, S.; Sasase, M.; Kamioka, H.; Kim, J.; Hosono, H. Lead-Free Highly Efficient Blue-Emitting Cs$_3$Cu$_2$I$_5$ with 0D Electronic Structure. *Adv. Mater.* **2018**, *30*, 1804547.

(22) Roccanova, R.; Yangui, A.; Nhalil, H.; Shi, H.; Du, M. H.; Saparov, B. Near-Unity Photoluminescence Quantum Yield in Blue-Emitting Cs$_3$Cu$_2$Br$_{5-x}$I$_x$ ($0 \leq x \leq 5$). *ACS Appl. Electron. Mater.* **2019**, *1*, 269−274.

(23) Zhou, C.; Tian, Y.; Yuan, Z.; Lin, H.; Chen, B.; Clark, R.; Dilbeck, T.; Zhou, Y.; Hurley, J.; Neu, J.; Besara, T.; Siegrist, T.;

Djurovich, P.; Ma, B. Highly Efficient Broadband Yellow Phosphor Based on Zero-Dimensional Tin Mixed-Halide Perovskite. *ACS Appl. Mater. Interfaces* **2017**, *9*, 44579−44583.

(24) Li, S.; Luo, J.; Tang, J.; Liu, J. Self-Trapped Excitons in All-Inorganic Halide Perovskites: Fundamentals, Status, and Potential Applications. *J. Phys. Chem. Lett.* **2019**, *10*, 1999−2007.

(25) Dong, Q.; Fang, Y.; Shao, Y.; Mulligan, P.; Qiu, J.; Cao, L.; Huang, J. Electron-hole Diffusion Lengths > 175 mm in Solution-grown CH$_3$NH$_3$PbI$_3$ Single Crystals. *Science* **2015**, *347*, 967−970.

(26) Shi, D.; Adinolfi, V.; Comin, R.; Yuan, M.; Alarousu, E.; Buin, A.; Chen, Y.; Hoogland, S.; Rothenberger, A.; Katsiev, K.; Losovyj, Y.; Zhang, X.; Dowben, P. A.; Mohammed, O. F.; Sargent, E. H.; Bakr, O. M. Low Trap-state Density and Long Carrier Diffusion in Organolead Trihalide Perovskite Single Crystals. *Science* **2015**, *347*, 519−522.

(27) Song, J.; Cui, Q.; Li, J.; Xu, J.; Wang, Y.; Xu, L.; Xue, J.; Dong, Y.; Tian, T.; Sun, H.; Zeng, H. Ultralarge All-Inorganic Perovskite Bulk Single Crystal for High-Performance Visible-Infrared Dual-Modal Photodetectors. *Adv. Opt. Mater.* **2017**, *5*, 1700157.

(28) Saidaminov, M. I.; Abdelhady, A. L.; Murali, B.; Alarousu, E.; Burlakov, V. M.; Peng, W.; Dursun, I.; Wang, L.; He, Y.; Maculan, G.; Goriely, A.; Wu, T.; Mohammed, O. F.; Bakr, O. M. High-quality Bulk Hybrid Perovskite Single Crystals within Minutes by InverseTemperature Crystallization. *Nat. Commun.* **2015**, *6*, 7586.

(29) Pan, W.; Wu, H.; Luo, J.; Deng, Z.; Ge, C.; Chen, C.; Jiang, X.; Yin, W.; Niu, G.; Zhu, L.; Yin, L.; Zhou, Y.; Xie, Q.; Ke, X.; Sui, M.; Tang, J. Cs$_2$AgBiBr$_6$ Single-crystal X-ray Detectors with a Low Detection Limit. *Nat. Photonics* **2017**, *11*, 726−732.

(30) Zeng, L. H.; Chen, Q. M.; Zhang, Z. X.; Wu, D.; Yuan, Y. Y.; Li, Y. Y.; Qarony, W.; Lau, S. P.; Luo, L. B.; Tsang, Y. H. Multilayered PtSe$_2$/Perovskite Schottky Junction for Fast, Self-Powered, Polarization-Sensitive, Broadband Photodetectors, and Image Sensor Application. *Adv. Sci.* **2019**, 1901134.

(31) Deng, W.; Zhang, X.; Huang, L.; Xu, X.; Wang, L.; Wang, J.; Shang, Q.; Lee, S. T.; Jie, J. S. Aligned Single-Crystalline Perovskite Microwire Arrays for High-Performance Flexible Image Sensors with Long-Term Stability. *Adv. Mater.* **2016**, *28*, 2201−2208.

(32) Zeng, L. H.; Wang, M. Z.; Hu, H.; Nie, B.; Yu, Y. Q.; Wu, C. Y.; Wang, L.; Hu, J. G.; Xie, C.; Liang, F. X.; Luo, L. B. Monolayer Graphene/Germanium Schottky Junction As High-Performance Self-Driven Infrared Light Photodetector. *ACS Appl. Mater. Interfaces* **2013**, *5*, 9362−9366.

(33) Boruah, B. D.; Mukherjee, A.; Misra, A. Sandwiched Assembly of ZnO Nanowires between Graphene Layers for a Self-powered and Fast Responsive Ultraviolet Photodetector. *Nanotechnology* **2016**, *27*, No. 095205.

(34) Kong, W. Y.; Wu, G. A.; Wang, K. Y.; Zhang, T. F.; Zou, Y. F.; Wang, D. D.; Luo, L. B. Graphene-β-Ga$_2$O$_3$ Heterojunction for Highly Sensitive Deep UV Photodetector Application. *Adv. Mater.* **2016**, *28*, 10725−10731.

(35) Lu, J.; Sheng, X.; Tong, G.; Yu, Z.; Sun, X.; Yu, L.; Xu, X.; Wang, J.; Xu, J.; Shi, Y.; Chen, K. Ultrafast Solar-Blind Ultraviolet Detection by Inorganic Perovskite CsPbX$_3$ Quantum Dots Radial Junction Architecture. *Adv. Mater.* **2017**, *29*, 1700400.

(36) Zhang, Q.; Jie, J.; Diao, S.; Shao, Z.; Zhang, Q.; Wang, L.; Deng, W.; Hu, W.; Xia, H.; Yuan, X.; Lee, S. T. Solution-Processed Graphene Quantum Dot Deep-UV Photodetectors. *ACS Nano* **2015**, *9*, 1561−1570.

(37) Chen, X.; Liu, K.; Zhang, Z.; Wang, C.; Li, B.; Zhao, H.; Zhao, D.; Shen, D. A Self-Powered Solar-Blind Photodetector with Fast Response Based on Au/beta-Ga$_2$O$_3$ Nanowires Array Film Schottky Junction. *ACS Appl. Mater. Interfaces* **2016**, *8*, 4185−4191.

(38) Xia, Y.; Zhai, G. M.; Zheng, Z.; Lian, L.; Liu, H.; Zhang, D. L.; Gao, J. B.; Zhai, T. Y.; Zhang, J. B. Solution-processed Solar-blind Deep Ultraviolet Photodetectors Based on Strongly Quantum Confined ZnS quantum dots. *J. Mater. Chem. C* **2018**, *6*, 11266−11271.

(39) Zhao, X.; Wu, Z.; Guo, D.; Cui, W.; Li, P.; An, Y.; Li, L.; Tang, W. Growth and Characterization of α-phase Ga$_{2−x}$Sn$_x$O$_3$ Thin Films for Solar-blind Ultraviolet Applications. *Semicond. Sci. Technol.* **2016**, *31*, No. 065010.